A depth migration method based on the full-wave reverse-time calculation and local one-way propagation

Xiao-Bi Xie and Ru-Shan Wu*
Institute of Geophysics and Planetary Physics, University of California at Santa Cruz

Summary

A depth migration method combining the full-wave reverse-time calculation and local one-way propagation is proposed. The full-wave finite-difference propagator is used to extrapolate the source and receiver waves in the model. The wavefields are extracted from selected locations and then a local one-way propagator is used to extrapolate the wavefield towards different directions. The one-way propagator is also served as a one-way filter, separating waves propagating along different directions. Finally, the image is calculated from directional waves generated by the one-way propagator and the artifacts from backscattered waves of both source and receiver sides are effectively eliminated. This method also dramatically reduces the size of output files which is important when dealing with large 3D models.

Introduction

The full-wave reverse-time migration method does not have the angle limitation of one-way propagators and can be used to image structures in complex areas especially for steeply dipping structures where turning waves are involved. Although the reverse-time migration is a relatively expensive method, the development of computer hardware and software (remarkably the popularities of PC clusters and Linux operating system) plus the ever increasing interests to explore complex structures in challenging regions stimulated recent interest to this method (e.g., Wu, et al., 1996; Mufti, et al., 1996; Sun and McMechanz, 2001; Biondi and Shan, 2002; Yoon, et al., 2003, 2004; Mulder and Plessix, 2004; Fletcher, et al., 2005; Wang, et al., 2005; Hou and Marfurt, 2005).

One of the major problems that affect the application of reverse-time migration is that the wide-angle capability of full-wave propagator can generate spurious cross correlations from diving waves and back-scattered waves, and causes serious artifacts (Yoon, et al., 2004; Mulder and Plessix, 2004; Fletcher, et al., 2005; Wang, et al., 2005). Special techniques such as velocity model smoothing or interface impedance matching have been introduced to solve this problem. These approaches can improve the situation in poststack migration where only one wavefield is involved, but the result is unsatisfied when applied to the prestack migration where cross correlation happens between the source and receiver waves.

Recently, several approaches have been proposed to solve this problem. Mulder and Plessix (2004) suggested that these artifacts can be removed by blanking the data, high-pass filtering or iterative migration. Yoon, et al. (2004) proposed to use an angle related weighting function calculated from Poynting vectors of source and receiver waves to pick the right events for imaging. Fletcher, et al. (2005) tried to eliminate the artifacts by introducing a directional damping term in areas where unwanted reflections occur. Wang et al. (2005) proposed a pseudo-space method by using a space distortion to transform a heterogeneous velocity model into a homogeneous model where no reflections were generated.

In this paper, we propose to use the local one-way propagator as the filter to separate the full-wave equation generated wavefield into directional waves. Then use directional wavefields for imaging. By making proper combinations of these directional waves, the artifacts caused by undesired waves can be avoided. Another advantage of this method is that it only needs to store part of the wavefield. The size of the file containing the wavefield can be reduced by about an order-of-magnitude which dramatically reduces the effort in input/output, network traffic and data management.

Methodology

The wavefield in a closed region without internal source can be calculated from its boundary values using the Rayleigh integral

$$u(\mathbf{r}) = \int_S \left(u(\boldsymbol{\xi}) \frac{\partial G(\mathbf{r},\boldsymbol{\xi})}{\partial n} - G(\mathbf{r},\boldsymbol{\xi}) \frac{\partial u(\boldsymbol{\xi})}{\partial n} \right) ds , \quad (1)$$

where $u(\mathbf{r})$ is the wavefield, $G(\mathbf{r},\boldsymbol{\xi})$ is the Green function, S is the boundary, $\mathbf{r}$ is the position of an internal point, $\boldsymbol{\xi}$ is the position on the boundary, and $\partial/\partial n$ is the derivative along the boundary normal. From the wavefield calculated using the full-wave propagator, choose the wavefield along certain boundaries, the wavefield in the entire region can be recovered from these boundary values. If we choose the boundaries along different directions and use one-way propagator as the Green function in equation (1), we can obtain waves propagating along different directions. For convenience, we use the wavefield on horizontal lines (or planes for 3D case) for wavefield extrapolation in near vertical direction and use wavefield on vertical lines for near horizontal extrapolation. By choosing different normal directions of

the boundary and using forward or backword one-way propagators, we can extrapolate wavefield in forward or backword directions.

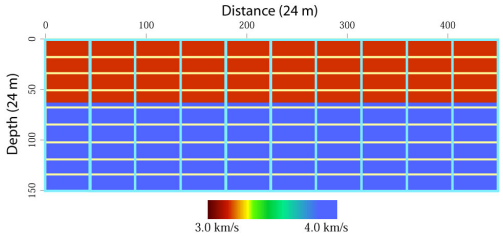

Figure 1. A simple two-layer velocity model. The horizontal and vertical lines indicate the locations where wavefields are needed for one-way extrapolations.

Taking the horizontal line as an example, the wavefield $u(\xi)$ and $\partial u(\xi)/\partial z$ are obtained from the full-wave calculation. Substituting these values into equation (1) and using one-way Green function $G^{+z}(\mathbf{r},\xi)$ and $\partial G^{+z}(\mathbf{r},\xi)/\partial z$, where superscript $+z$ denotes the one-way propagator along positive z direction, we can calculate wavefield below that horizontal line. Similarly, using Green function $G^{-z}(\mathbf{r},\xi)$ and $\partial G^{-z}(\mathbf{r},\xi)/\partial z$, we can calculate wavefield above the horizontal line and along $-z$ direction. Using wavefield along horizontal lines at different depth levels, we can reconstruct wavefields along $+z$ and $-z$ directions between these lines. A similar method can be used to process the near horizontally propagating waves. In these cases, the one-way propagator only deals with narrow-angle propagation and the wavefield is extrapolated only for a very short distance. The accuracy of the one-way propagator will not seriously affect the result.

Numerical Examples

To show how this system works, we first conduct the migration for a simple two-layer model. Figure 1 shows the velocity model. The size of the model is 451×150 with $dx = dz = 24\,\text{m}$, and the velocities are 3.0 km/s and 4.0 km/s for upper and lower layers, respectively. The horizontal and vertical lines in the velocity model indicate the location where the wavefield is picked. Both the synthetic data and the reverse-time migration are calculated using a fourth-order full-wave finite-difference code. To focus our attention to the effect of back-scattered waves, We mute the first arrival from the shot record. Shown in Figure 2 is migrated wavefield using the full-wave method, with 2a and 2b are source waves at 0.8 s and 1.2 s, and 2c and 2d are receiver waves at $T-0.8\text{s}$ and $T-1.2\text{s}$, where T is the maximum recording time. We then output the wavefield on horizontal lines at depths for every 15 dz and use a one-way propagator (Xie and Wu, 1998, 2005) to extrapolate the wavefield from each depth to the next depth (15 steps). Figures 3a and 3b are the reconstructed wavefield $u_s^{+z}(\mathbf{r})$, and 3c and 3d are the reconstructed wavefield $u_g^{-z}(\mathbf{r})$, where subscripts s and g denote source and receiver waves. Compared with Figure 2, the undesired reflections have been eliminated.

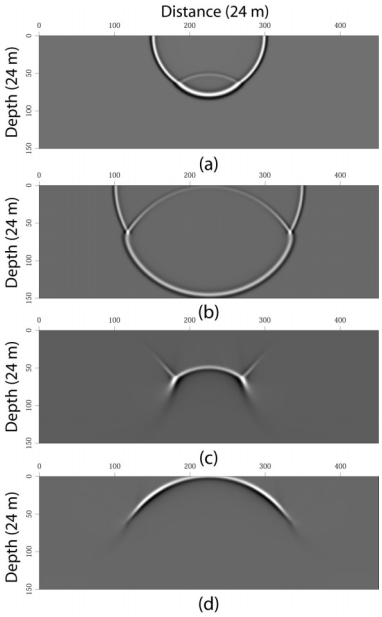

Figure 2. Wavefield snapshots calculated using full-wave finite-difference method. (a) and (b) are source wavefields at 0.8 s and 1.2 s. (c) and (d) are receiver wavefields at $T-0.8\text{s}$ and $T-1.2\text{s}$.

The image can be calculated from directional wavefields. To avoid artifacts from cross correlations between diving waves and back-scattered waves, we choose wave pairs related to the true reflections, for example $u_s^{-z}(\mathbf{r})u_g^{+z}(\mathbf{r})$, $u_s^{+z}(\mathbf{r})u_g^{-z}(\mathbf{r})$, $u_s^{+x}(\mathbf{r})u_g^{-x}(\mathbf{r})$ or $u_s^{-x}(\mathbf{r})u_g^{+x}(\mathbf{r})$, to form the image. The final image can be obtained by summing up all partial images. Shown in Figure 4 are reverse-time images for the two-layer model, where 4a is calculated using the conventional zero-lag cross correlation image condition

$$I(\mathbf{r}) = \int_0^T u_s(\mathbf{r},t)u_g(\mathbf{r},T-t)\,dt\,, \qquad (2)$$

where $I(\mathbf{r})$ is the image, u_s and u_g are source and receiver waves. Figure 4b is calculated using the image condition given by Yoon et al. (2004). In Figure 4c, the image is calculated from directional waves

$u_s^{+z}(\mathbf{r},t)u_g^{-z}(\mathbf{r},T-t)$ reconstructed using local one-way propagator. In Figure 4a, there are artifacts shown above the interface, while in 4b and 4c, they have been properly removed.

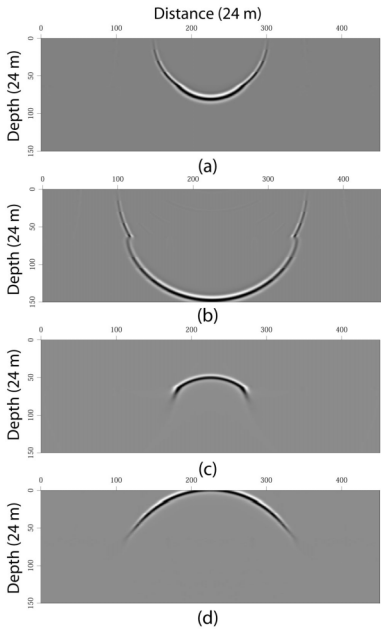

Figure 3. Wavefield snapshots reconstrcted using the one-way propagator. (a) and (b) are wavefields along $+z$ and at 0.8 s and 1.2 s. (c) and (d) are wavefields along $-z$ and at $T-0.8\text{s}$ and $T-1.2\text{s}$. Note that compared with the finite-difference result shown in Figure 2, the undesired reflections have been eliminated.

As second example, we calculate the image of a simple salt dome model. Figure 5 shows the velocity model overlapped with the wavefield snapshot from the finite-difference forward modeling. The velocity model composed of a background with a vertical velocity gradient and a salt dome with steep flanks. The size of the model is the same as the two-layer model and reflections from different part of the structure are indicated with rays. To image the steep flank of the salt dome, wide angle turning waves must be properly handled.

Figure 6 shows the images from depth migrations overlapped with the velocity model. A single source is used to illuminate the model. Figure 6a is calculated using the conventional zero-lag cross correlation imaging condition. Figure 6b is calculated using the imaging condition of Yoon et al. (2004). Figure 6c is calculated from the waves $u_s^{+z}(\mathbf{r})$ and $u_g^{-z}(\mathbf{r})$ reconstructed using the local one-way propagator, and 6d is calculated using $u_s^{+x}(\mathbf{r})$ and $u_g^{-x}(\mathbf{r})$.

Note that horizontal structure is better imaged in 6c and vertical structure is better imaged in 6d. The artifacts shown in 6a have been removed in 6b to 6d.

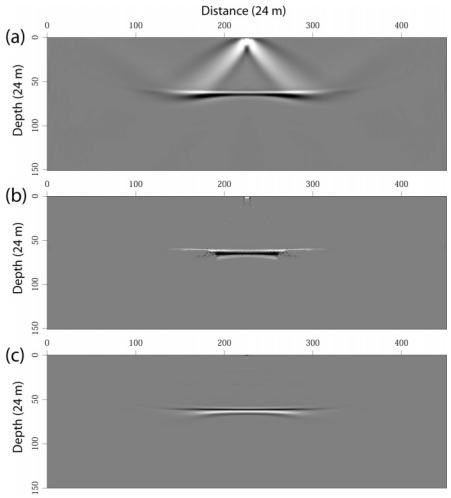

Figure 4. Reverse-time images for the two-layer model, (a) using conventional zero-lag image condition, (b) using the image condition given by Yoon et al. (2004), and (c) using full-wave propagator plus local one-way propagator.

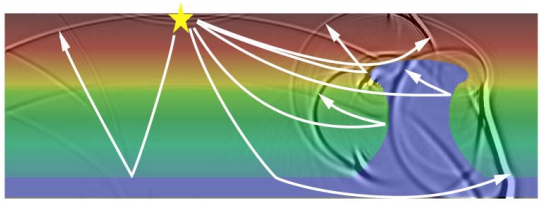

Figure 5. A simple salt dome model with steep flanks. Overlapped is the snapshot generated by finite-difference forward modeling. The major reflection events are marked with rays.

Discussions and Conclusion

We proposed a depth migration method based on the full-wave reverse-time calculation and local one-way propagation. Both the source and receiver waves are extrapolated using the full-wave finite-difference propagator. There is no angle limitation for these wavefields. Then the local one-way propagator is used to separate the waves into different directions. Finally, the image is calculated using directional wavefields. Using the one-way propagator at the imaging stage has the following advantages. (i) It eliminates undesired waves and removes the artifacts. (ii) The input/output file size can be substantially reduced (about an order-of-magnitude smaller than if the entire wavefield is dumped out). The additional computation for the one-way propagation can be

compensated by the time saved from the I/O and network traffic. The reduced file size makes the management of the data easier and provides the possibility for repeated later studies.

The result presented in this paper is preliminary. Further investigation is needed to better reconstruct the wavefield in complex regions using one-way propagator. More sophisticated method such as the angle domain image analysis (Wu, et al. 2004, and Xie, et al., 2005) may be required to combine images from multi-directional wavefileds.

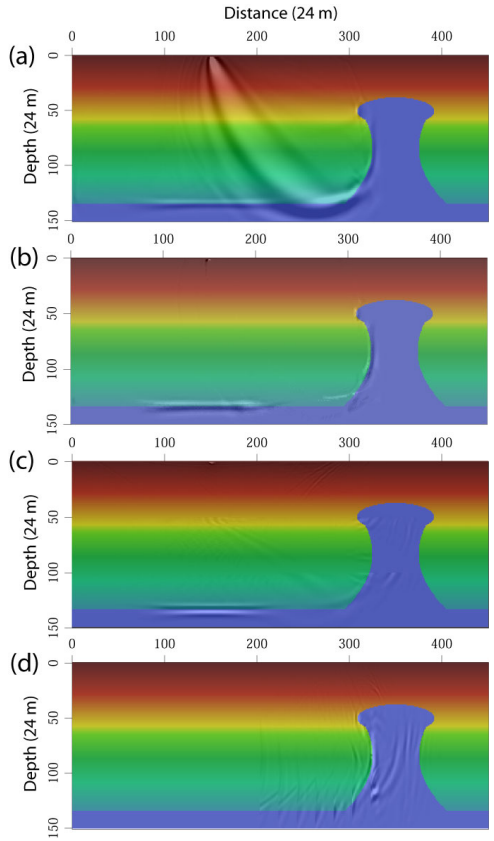

Figure 6. Depth migration image for a simple sand dome model, (a) using the conventional zero-lag imaging condition, (b) using the image condition of Yoon et al. (2004), (c) using $u_s^{+z}(\mathbf{r})u_g^{-z}(\mathbf{r})$ and (d) using $u_s^{+x}(\mathbf{r})u_g^{-x}(\mathbf{r})$.

Acknowledgement. This research is supported by the DOE/BES project at the University of California, Santa Cruz under the Grant No. DE-FG02-04ER15530. The facility support from the W.M. Keck Foundation is also acknowledged.

References

Biondi, B. and G. Shan, 2002, Prestack imaging of overturned reflections by reverse time migration: 72nd Annual International Meeting, SEG, Expanded Abstracts, 1284-1287.

Fletcher, R.F., P. Fowler, P. Kitchenside, and U. Albertin, 2005, Suppressing artifacts in prestack reverse time migration: 75th Annual International Meeting, SEG, Expanded Abstracts, 2049-2052.

Hou, A., and K. Marfurt, 2005, 3D PSDW prestack depth migration: 75th Annual International Meeting, SEG, Expanded Abstracts, 1818-1821.

Mufti, I.R. J.A. Pita, and R.W. Huntley, 1996, Finite-difference depth migration of exploration-scale 3-D seismic data: Geophysics, **61**, 776-794.

Mulder, W.A., and R.E. Plessix, 2004, A comparison between one-way and two-way wave-equation migration: Geophysics, **69**, 1491-1504.

Sun, R., and G.A. McMechanz, 2001, Scalar reverse-time depth migration of prestack elastic seismic data: Geophysics, **66**, 1519-1527.

Wang, X., D. Xia, J. Li, Q. Tang and X. Jiang, 2005, Model based processing (III): pseudo-space reverse time migration: 75th Annual International Meeting, SEG, Expanded abstracts, 2261-2264.

Wu, R.S., Chen, S. and Luo, M., 2004, Migration amplitude correction in angle domain using beamlet decomposition: Expanded abstracts, EAGE 66th Annual Meeting.

Wu, W.J., L.R. Line, and H.X. Lu, 1996. Analysis of higher-order, finite-difference schemes in 3-D reverse-time migration: Geophysics, 61, 845-856.

Xie, X.B., and R.S. Wu, 1998, Improve the wide-angle accuracy of screen method under large contrast: 68th Annual International Meeting, SEG, Expanded Abstracts, 1811-1814.

Xie, X. B., and R. S. Wu, 2005, Multicomponent prestack depth migration using elastic screen method: Geophysics, **70**, S30-S37.

Xie, X.B., Wu, R.S., M.Fehler and L. Huang, 2005, Seismic resolution and illumination: A wave-equation-based analysis: 75th Annual International Meeting, SEG, Expanded abstracts, 1862-1865.

Yoon, K., C. Shin, S. Suh, L. Lines, S.H., Kigam, 2003, 3D reverse-time migration using the acoustic wave equation: An experience with the SEG/EAGE data set: The Leading Edge, **22**, 38-41.

Yoon, K., K.J. Marfurt, and W. Starr, 2004, Challenges in reverse-time migration: 74th Annual International Meeting, SEG, Expanded Abstracts, 1057-1060.

EDITED REFERENCES

Note: This reference list is a copy-edited version of the reference list submitted by the author. Reference lists for the 2006 SEG Technical Program Expanded Abstracts have been copy edited so that references provided with the online metadata for each paper will achieve a high degree of linking to cited sources that appear on the Web.

REFERENCES

Biondi, B., and G. Shan, 2002, Prestack imaging of overturned reflections by reverse time migration: 72nd Annual International Meeting, SEG, Expanded Abstracts, 1284–1287.

Fletcher, R. F., P. Fowler, P. Kitchenside, and U. Albertin, 2005, Suppressing artifacts in prestack reverse time migration: 75th Annual International Meeting, SEG, Expanded Abstracts, 2049–2052.

Hou, A., and K. Marfurt, 2005, 3D PSDW prestack depth migration: 75th Annual International Meeting, SEG, Expanded Abstracts, 1818–1821.

Mufti, I. R., J. A. Pita, and R. W. Huntley, 1996, Finitedifference depth migration of exploration-scale 3-D seismic data: Geophysics, **61**, 776–794.

Mulder, W. A., and R. E. Plessix, 2004, A comparison between one-way and two-way wave-equation migration: Geophysics, **69**, 1491–1504.

Sun, R., and G. A. McMechanz, 2001, Scalar reverse-time depth migration of prestack elastic seismic data: Geophysics, **66**, 1519–1527.

Wang, X., D. Xia, J. Li, Q. Tang, and X. Jiang, 2005, Model based processing (III): pseudo-space reverse time migration: 75th Annual International Meeting, SEG, Expanded abstracts, 2261–2264.

Wu, R. S., S. Chen, and M. Luo, 2004, Migration amplitude correction in angle domain using beamlet decomposition: 66th Annual Conference and Exhibition, EAGE, Extended Abstracts, G029.

Wu, W. J., L. R. Line, and H. X. Lu, 1996, Analysis of higher-order, finite-difference schemes in 3-D reverse-time migration: Geophysics, **61**, 845–856.

Xie, X. B., and R. S. Wu, 1998, Improve the wide-angle accuracy of screen method under large contrast: 68th Annual International Meeting, SEG, Expanded Abstracts, 1811–1814.

———, 2005, Multicomponent prestack depth migration using elastic screen method: Geophysics, **70**, S30–S37.

Xie, X. B., R. S. Wu, M. Fehler, and L. Huang, 2005, Seismic resolution and illumination: A waveequation-based analysis: 75th Annual International Meeting, SEG, Expanded abstracts, 1862–1865.

Yoon, K., K. J. Marfurt, and W. Starr, 2004, Challenges in reverse-time migration: 74th Annual International Meeting, SEG, Expanded Abstracts, 1057–1060.

Yoon, K., C. Shin, S. Suh, L. Lines, and S. H., Kigam, 2003, 3D reverse-time migration using the acoustic wave equation: An experience with the SEG/EAGE data set: The Leading Edge, **22**, 38–41.